Effects of strain rate on mode II interlaminar fracture toughness in carbon-fibre/epoxy laminated composites

T. Kusaka, Y. Yamauchi, T. Kurokawa

JOURNAL DE PHYSIQUE IV
Colloque C8, supplément au Journal de Physique III, Volume 4, septembre 1994

Effects of strain rate on mode II interlaminar fracture toughness in carbon-fibre/epoxy laminated composites

T. Kusaka, Y. Yamauchi* and T. Kurokawa**

Hyogo Prefectural Institute of Industrial Research, 3-1-12 Yukihira-cho, Suma-ku Kobe 654, Japan
** Dept. of Precision Engineering, Osaka University, 2-1 Yamadaoka Suita 565, Japan*
*** Dept. of Aeronautical Engineering, Kyoto University, Yoshidahonmachi, Sakyo-ku, Kyoto 606-01, Japan*

Résumé: La relation entre la vitesse de déformation et la résistance à la rupture interlaminaire en Mode II d'un composite laminé CF/epoxy a été examiné par des experiences en flexion d'un composite prédelaminé à son extremité en mode dynamique (dynamic ENF test) utilisant l'essai SHPB. Les ondes incidentes de forme exponentielle ont évité le problème de vibrations parasites en flexion. L'analyse dynamique par les éléments finis confirme que la formule estimée peut être utilisée pour la r'esistance à la rupture Mode II, aussi bien en dynamique qu'en statique. Les résultats expérimentaux montrent que la résistance à la rupture en Mode II a tendance à diminuer avec l'accroissement de la vitesse de déformation en cisaillement. Ceci serait dû aux différences entre ruptures dynamique et statique.

Abstract: The strain rate dependence of Mode II interlaminar fracture toughness in unidirectional CF/epoxy composite laminates was studied by the dynamic End Notched Flexure (ENF) test using a Split Hopkinson Pressure Bar (SHPB) system. The experimental technique using a ramped incident wave was adopted to suppress the influence of the flexural vibration of the specimen. Finite element analysis confirmed that the estimating formula for static Mode II fracture toughness can be applied to dynamic Mode II fracture toughness as well. The experimental results indicated that the Mode II fracture toughness tends to decrease with increasing shear strain rate. This tendency is thought to be due to the fractographic differences between static and dynamic fractures.

1. INTRODUCTION

In composite structures, the small delamination cracks introduced during manufacturing or working processes can cause catastrophic failure. Recently, many studies applying linear fracture mechanics to this kind of problem have been conducted, and the DCB (Double Cantilever Beam) test for the opening mode (Mode I), the ENF (End Notched Flexure) test[1,2] for the shearing mode (Mode II) and the CLS (Cracked Lap Shear) test for the mixture of Modes I and II have been performed as standard experimental methods. Applying these, the interlaminar fracture toughness and the crack propagation behaviour under static loading have been studied in various kinds of composite laminate. But relatively few experimental results under dynamic or impact loading have been reported[3,4]. In the present study, the SHPB (Split Hopkinson Pressure Bar) technique was employed to carry out dynamic ENF tests, and the strain rate dependence of Mode II interlaminar fracture toughness in two typical unidirectional CF/epoxy composites was investigated.

2. EXPERIMENTAL PROCEDURE

2.1 Static ENF Test

Static ENF tests were carried out at shear strain rates ranging from 10^{-5} to 10^{-1} sec^{-1} using universal testing instruments. The ENF test is one of the most general methods for measuring Mode II interlaminar fracture toughness in composite laminates. As shown in Figure 1, it is essentially

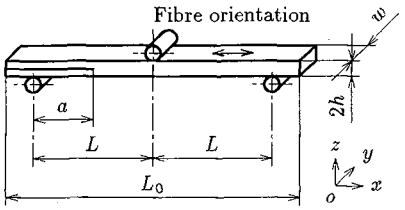

Figure 1: End notched flexure specimen.

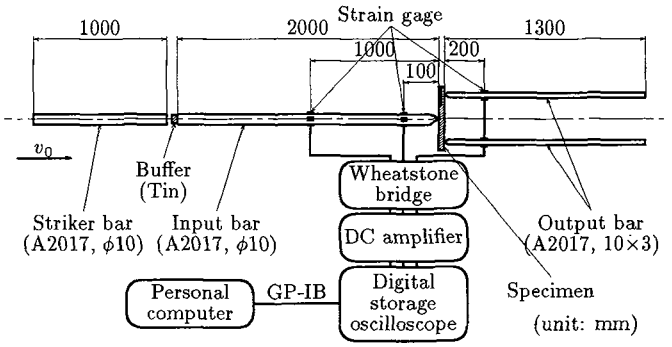

Figure 2: Dynamic ENF test apparatus.

a three-point flexure test using a coupon specimen with an embedded through-width delamination placed at the laminate midsurface where the interlaminar shear stress is greatest; Gillespie et al.[1] have proved by FEM analysis that the ENF test is a pure Mode II fracture test within the limits of small deformation.

2.2 Dynamic ENF Test

Dynamic ENF tests were carried out at shear strain rates ranging from 10^1 to 10^2 sec^{-1} using the SHPB system as shown in Figure 2. The experimental technique placing a soft metal buffer on the collision face between the striker bar and the input bar was used. This was effective to generate a ramped incident wave and to suppress the high frequency vibration of the specimen at the early stage of loading. A few examples of histories of ramped incident waves are shown later in Figure 6 (a).

2.3 Specimen Preparation

Two typical CF/epoxy composite materials were examined in the present study. One is T300/2500 (Toray), which has a standard epoxy matrix of 100 MPa in strength. The other is Q-C133 (Toho rayon), which has a toughened epoxy matrix of 140 MPa in strength by containing a thermoplastic resin. The T300/2500 panels were processed in a heat press and the Q-C133 panels were processed in an autoclave according to the manufacturers' recommended cure cycles (Q-C133: at 180 °C, T300/2500: at 120 °C). Both were machined to specimens with a diamond saw with the geometries shown in Table 1. The initial cracks were introduced by inserting a 25 μm thick Teflon film in the lay-up process and precracked with a cutter blade to avoid the influence of the resin-rich region at the film's tip.

Table 1: Mechanical properties and geometries of the ENF specimen.

	Young's mod. E_x (GPa)	Shear mod. G_{xy} (GPa)	Volume frac. V_f (%)	Stacking sequence	Dimensions (mm)				
					$2L$	$2h$	w	a	L_0
Q-C133	140	4.0	54	$[0^\circ_{20}]$	60	2.6	5	15	70
T300/2500	120	3.2	56	$[0^\circ_{40}]$	30	5.1	5	7.5	40

3. DATA REDUCTION

3.1 Load

The applied load history at the centre of the specimen, $P_{cnt}(t)$, and the reaction force history at the two supporting points of the specimen, $P_{sup}(t)$, are given by,

$$P_{cnt}(t) = (\sigma_I(t) + \sigma_R(t)) \cdot A_{inp}\,, \qquad P_{sup}(t) = \sigma_T(t) \cdot A_{out} \tag{1}$$

where $\sigma_I(t)$ and $\sigma_R(t)$ are the histories of the incident and reflected stress waves in the input bar, and $\sigma_T(t)$ is the sum of the transmitted stress waves in the two output bars (compressive stress and load are defined to be positive in this paper), and A_{inp} and A_{out} are the cross sectional area of the

input and output bars. Typical histories of $P_{cnt}(t)$ and $P_{sup}(t)$ are shown in Figure 3. Generally the equilibrium of these forces does not hold good in dynamic tests, unlike static tests, because of inertia forces. However, utilizing a ramped incident wave, the influence of the inertia force becomes small and the difference between $P_{cnt}(t)$ and $P_{sup}(t)$ can be supposed to be negligible near the time of fracture initiation. Thus the load applied to the specimen, $P(t)$, can be approximated by,

$$P(t) \simeq P_{cnt}(t) \simeq P_{sup}(t) \tag{2}$$

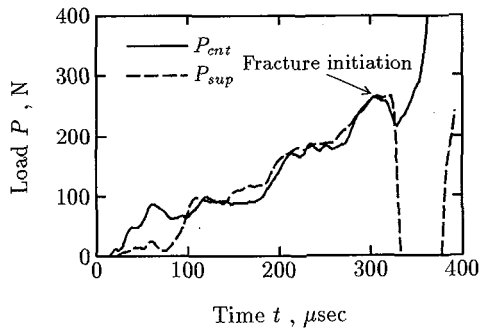

Figure 3: Histories of the applied load, P_{cnt}, and the reaction force, P_{sup}, in a dynamic ENF test.

3.2 Displacement

In accordance with one-dimensional elastic wave theory, the particle velocities at the right end of the input bar, $v_{inp}(t)$, and at the left end of the output bars, $v_{out}(t)$, are given by,

$$v_{inp}(t) = \frac{\sigma_I(t) - \sigma_R(t)}{\rho_{inp} c_{inp}}, \qquad v_{out}(t) = \frac{\sigma_T(t)}{\rho_{out} c_{out}} \tag{3}$$

where $\rho_{inp}c_{inp}$ and $\rho_{out}c_{out}$ are the acoustic impedances of the input and output bars. Except at the early stage of loading, the specimen can be considered to keep contact with the input bar and the output bars because the values of $P_{cnt}(t)$ and $P_{sup}(t)$ are not zero. Thus the total deflection of the specimen, $\delta(t)$, is,

$$\delta(t) = \int (v_{inp}(t) - v_{out}(t))\, dt \tag{4}$$

3.3 Mode II Static Fracture Toughness

Using the compliance technique based on Griffith's fracture criteria, the static energy release rate, G, is given by[5],

$$G = \frac{P^2}{2} \cdot \frac{dC}{dA} \tag{5}$$

where C is the compliance of the specimen and A is the area of the crack. Calculating the value of C theoretically, the Mode II critical energy release rate, G_{IIC}, is reduced to,

$$G_{IIC}^{SH} = \frac{9a^2 P_C^2}{16 E_x w^2 h^3} \left\{ 1 + 0.2 \frac{E_x}{G_{xz}} \left(\frac{h}{a} \right)^2 \right\} \tag{6}$$

or,

$$G_{IIC}^{PT} = \frac{9a^2 P_C^2}{16 E_x w^2 h^3} \left\{ 1 + \frac{\alpha}{3} \sqrt{\frac{E_x}{G_{xz}}} \left(\frac{h}{a} \right) + \frac{\alpha^2}{30} \frac{E_x}{G_{xz}} \left(\frac{h}{a} \right)^2 \right\} \tag{7}$$

where w, h, a, E_x and G_{xz} are the width, the half of thickness, the initial crack length, the Young's modulus and the shear modulus of the specimen, respectively. P_C is the load at fracture initiation; here, P_C was considered as the maximum value of applied load because the matrixes of the present materials were relatively brittle and fracture grows unstably[2]. The constant, α, can be determined by FEM analysis. Equation (6) is based on beam theory with shear deformation included[2] and applied to the specimens of Q-C133, and Equation (7) is based on plate theory[5] and applied to the specimens of T300/2500, whose values of h/a were comparatively large.

3.4 Mode II Dynamic Fracture Toughness

In dynamic ENF tests, the following two points must be taken into account when estimating the value of G_{IIC} by the compliance technique; firstly the dynamic deformation mode of the specimen is generally different from the static mode; secondly the kinetic energy of the specimen may affect

the estimation of the dynamic fracture toughness. With respect to the first problem, the dynamic deformation mode was the same as the static mode within the present experimental conditions, as is discussed in the next section. With respect to the second problem, Smiley et al.[3] have estimated the kinetic energy contribution from,

$$G_{IIC}^{dyna} = G_{IIC}^{stat} + 0.078\rho h\dot{\delta}^2 \tag{8}$$

where G_{IIC}^{dyna} is a true dynamic fracture toughness and G_{IIC}^{stat} is the apparent fracture toughness evaluated by Equation (6) or (7) derived by the compliance technique. The second term of the right-hand side ranged from 0.2 to 3 % in the present specimens, so its influence was neglected and the equation estimating G_{IIC}^{stat} was applied to estimate the value of G_{IIC}^{dyna} as well. The validity of this approximation will be confirmed in the next section by means of FEM analysis.

3.5 Shear Strain Rate

To discuss the dynamic properties of materials, a parameter indicating the rate of deformation should be defined. Here, the shear strain rate at the midsurface of the specimen, $\dot{\gamma}(t)$, was used and estimated by,

$$\dot{\gamma}(t) = \frac{3\dot{P}(t)}{8G_{xz}wh} \tag{9}$$

4. RESULTS AND DISCUSSION

4.1 Load-Displacement Response

A typical load-displacement curve reduced by the above procedures in a dynamic ENF test is shown in Figure 4. The solid line shows an experimental load-displacement curve and the dotted line shows the theoretical curve evaluated by static beam theory. The experimental curve shows overall agreement with the static theoretical curve except for some oscillation. Therefore the dynamic deformation mode can be considered to be the same as the static mode. It is valid, therefore, to calculate the compliance of the specimen by static beam or plate theory.

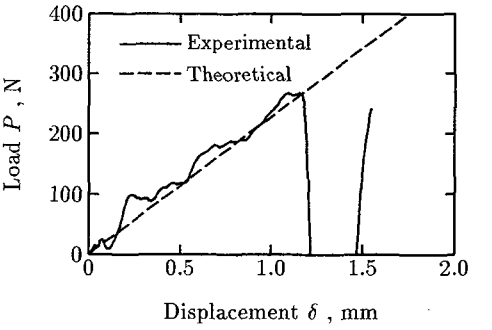

Figure 4: Load-displacement response in a dynamic ENF test.

4.2 Computational Approach

From Irwin's theory of fracture[7], the energy absorbed in the process of crack growth is equal to the amount of work required to close the crack to its original length. This theory is very convenient to FEM analysis and used as virtual crack closure technique[8]. When the crack is modeled in two-dimensional elements as shown in Figure 5, the Mode II energy release rate, G_{II}^{CC}, is given by,

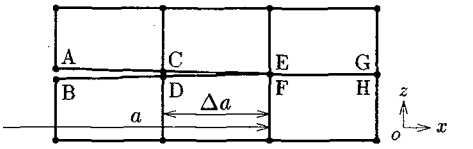

Figure 5: Finite element model at the crack tip.

$$G_{II}^{CC} = \frac{1}{2w\Delta a} T_E(u_C - u_D) \tag{10}$$

where T_E is the x-component of the nodal force at the node E, and u_C and u_D are the x-components of the displacement of the nodes C and D. This formula can evaluate Mode II energy release rate directly without the need to consider the dynamic deformation mode of the specimen. In the present study, the dynamic ENF test was simulated by this method. Some examples of calculated results for reciprocal G_{II}^{PT} histories nondimensionalized by G_{II}^{CC} are shown in Figure 6 (b), where G_{II}^{PT} is the apparent energy release rate evaluated by Equation (7) and the incident waves were assumed to have the ramped velocity form shown by the thick solid lines in Figure 6 (a) and given by,

$$V(t) = V_0\left\{1 - \exp\left(-\frac{t^2}{T^2}\right)\right\} \tag{11}$$

where T is a rise-time parameter. In Figure 6 (a), the thin solid and dotted lines show the experimental incident waves with and without a soft metal buffer, respectively. Figure 6 (b) shows that the value of G_{II}^{PT} converges into the value of G_{II}^{CC} for $T \geq 30$ after $t = 100$ μsec. Hence the static formula derived from the compliance technique can also be applied to estimate the dynamic fracture toughness if a ramped incident wave is applied.

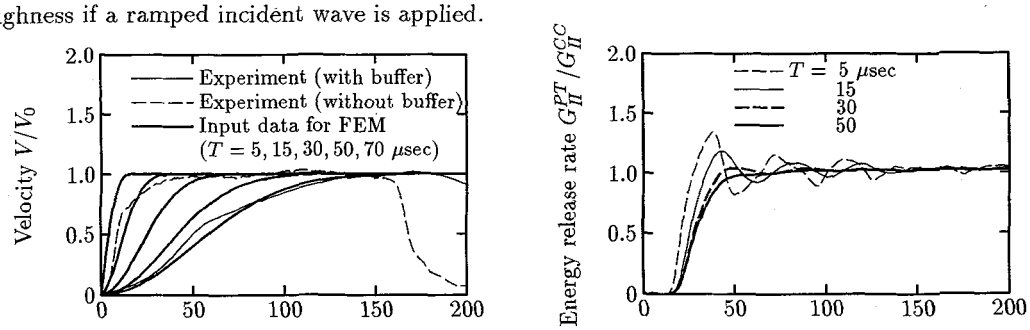

(a) Incident waves (b) Energy release rate

Figure 6: Incident wave histories with various rise-times and histories of the dynamic energy release rate, G_{II}^{PT}, by FEM.

4.3 Effects of Strain Rate

The relationship between the fracture toughness, G_{IIC}, and the shear strain rate at crack initiation, $\dot{\gamma}_C$, is shown in Figure 7, where ○, ● and ◇ are the data in Q-C133, T300/2500 and AS4/2220-3[4], respectively. Figure 7 indicates that the Mode II fracture toughness tends to decrease with increasing shear strain rate and that the value of G_{IIC} at $\dot{\gamma}_C = 10^2$ sec^{-1} is approximately 20 % lower than the value at $\dot{\gamma}_C = 10^{-5}$ sec^{-1} in each material equally.

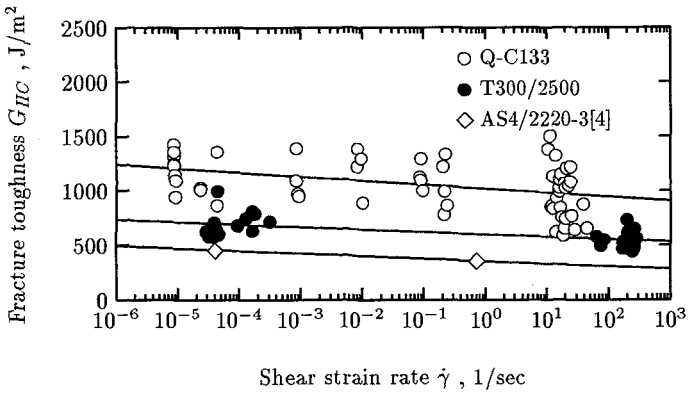

Figure 7: Strain rate effects on Mode II fracture toughness.

4.4 Fractography

Figure 8 shows delamination surfaces in the ENF specimens at a distance of 1 mm from the initial crack tip observed with a SEM; (a) is a static fracture surface ($\dot{\gamma}_C = 9.2 \times 10^{-6}$ sec^{-1}) and (b) is a dynamic fracture surface ($\dot{\gamma}_C = 3.8 \times 10^{1}$ sec^{-1}), and the crack propagated from the top to the bottom. The hackle-looking fracture surfaces due to ductile fracture in the matrix resin are observed at low strain rates. The smooth fracture surfaces due to debonding at the interface between reinforcing fibres and matrix resin are mainly observed, and the matrix resin is only deformed a little,

at high strain rates. These fractographic differences are supposed to have much to do with the above tendency, that is, the dynamic strength of bonding between reinforcing fibres and matrix resin may be lower than the static strength. The fibre surfaces of both materials were treated in standard processes, but the influence of the surface treatment on the dynamic strength has not been clear yet.

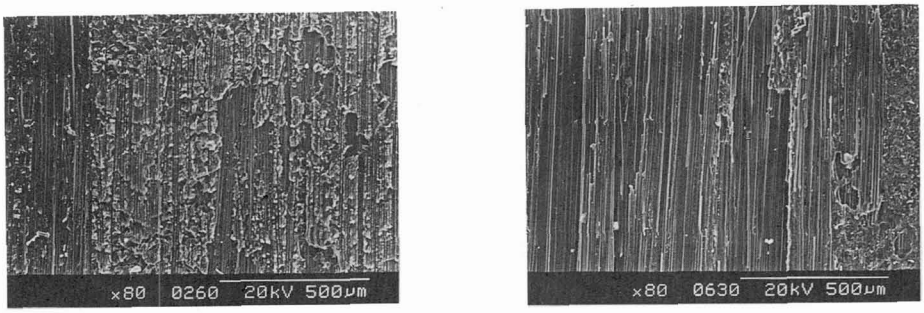

(a) Static (b) Dynamic

Figure 8: Typical fracture surfaces in Q-C133.

5. SUMMARY AND CONCLUSIONS

Dynamic ENF tests were performed in unidirectional CF/epoxy composite laminates using the SHPB system in order to estimate the Mode II interlaminar fracture toughness at high strain rates. It has been shown that the Mode II dynamic interlaminar fracture toughness can be estimated by means of the compliance technique based on beam or plate theory as in the case of static ENF tests if a ramped incident wave with an appropriate rise-time is applied, thereby suppressing the high frequency flexural vibration of the specimen. This was confirmed by the FEM analysis using the virtual crack closure technique.

Using the above procedures, the strain rate dependence of Mode II interlaminar fracture toughness in two typical CF/epoxy composites was investigated. The results indicated that the Mode II interlaminar fracture toughness tends to decrease with increasing strain rate; the fracture toughness, G_{IIC}, at the shear strain rate $\dot{\gamma}_C = 10^2$ sec^{-1} was approximately 20 % lower than the value at $\dot{\gamma}_C = 10^{-5}$ sec^{-1} in each material.

The SEM observations indicated that the above tendency is caused by the fractographic differences; the hackle-looking fracture surfaces due to ductile fracture in the matrix resin are observed at low strain rates, but the smooth fracture surfaces due to debonding at the interface between reiforcing fibres and the matrix resin are mainly observed at high strain rates.

REFERENCES

[1] Gillespie J. W. Jr., Carlsson L. A. and Pipes R. B., *Comp. Sci. & Tech.* **26** (1986) 177-197.

[2] Carlsson L. A., Gillespie J. W. Jr. and Pipes R. B., *J. Comp. Mat.* **20** (1986) 594-605.

[3] Smiley A. J. and Pipes R. B., *Comp. Sci. & Tech.* **29** (1987) 1-15.

[4] Maikuma H., Gillespie J. W. Jr. and Wilkins D. J., *J. Comp. Mat.* **24** (1990) 124-149.

[5] Carlsson L. A. and Pipes R. B., Experimental Characterization of Advanced Composite Materials (Prentice-Hall, New York, 1987) Chap. 2.

[6] Carlsson L. A., Gillespie J. W. Jr. and Whitney J. M., Proc. 1st Conf. on Comp. Mat., (Technomic Publishing, 1986) pp.421.

[7] Irwin G. R., Handbuch der Physik (Flügge Edition, Berlin, 1958) pp.551.

[8] Rybicki E. F. and Kanninen M. F., *Eng. Fracture Mech.* **9** (1977) 931.